Southern California Edison Company

P. O. BOX 800
2244 WALNUT GROVE AVENUE
ROSEMEAD, CALIFORNIA 91770

K. P. BASKIN
ER OF NUCLEAR ENGINEERING,
AFETY, AND LICENSING

TELEPHONE
(213) 572-1401

December 9, 1980

Director, Office of Nuclear Reactor Regulation
Attention: Mr. Frank Miraglia, Branch Chief
Licensing Projects Branch 3, DPM
U. S. Nuclear Regulatory Commission
Washington, D.C. 20555

Gentlemen:

Subject: Docket Nos. 50-361 and 50-362
San Onofre Nuclear Generating Station
Units 2&3

In response to a request for additional information by the NRC Structural Engineering Branch, enclosed are 63 (sixty-three) copies of clarifications, references and a revised Section 4.0 of the report, "Water Tight Reliability of Condensate Storage Tank and Its Concrete Enclosure Walls under DBE and Tornado Event." This report, referenced in the response to NRC Question 010.65, was submitted to the NRC by letter dated September 29, 1980.

Please let me know if you have any further questions concerning this report.

Very truly yours,

K P Baskin

Enclosures

B201
S
1/63

SUPPLEMENTAL INFORMATION

TO

"WATER TIGHT RELIABILITY OF CONDENSATE STORAGE TANK AND ITS CONCRETE ENCLOSURE WALLS UNDER DBE AND TORNADO EVENT" DATED SEPTEMBER 29, 1980

December 1980

CONTENTS

4.0 Technical Approach and Basis for Leakage Analysis

The leakage calculation is based on theoretical expressions for flow through parallel plates extended to model flow through cracks in the reinforced concrete walls. A summary of the deriviation of the equations is outlined on Table 4.1. The application of equation (7) of Table 4.1 requires that the actual crack pattern be represented by horizontal cracks. However, the actual cracks are of complex cross section and of variable aperture, therefore, equivalent constant apertures of cracks are calculated by the relationships summarized on Table 4.2.[4] and Appendix B. The vertical cracks were modeled as equally dimensioned horizontal cracks at elevations 16.7, 11, and 6.2 ft. For example, as shown on Fig. 4-1 the 5.8 ft. segment of each vertical crack from the water surface (elevation 22.5 ft.) to elevation 16.7 ft. was taken as a 5.8 ft. long horizontal crack at elevation 16.7 ft. Similarly, the segment of each vertical crack between elevation 16.7 and 11 ft. was taken as a 5.7 ft. long crack at elevation 11 ft., etc. By considering the equivalent horizontal cracks as located at the lowest level of each vertical segment larger applicable heads result, and a conservatively larger flow quantity is thereby calculated. Use of this conservative procedure considerably simplified the calculations while maintaining the conservatism. The leakage in the room can then be calculated in increments using equation (7) of Table 4.1.

4.1 Discussion of the Basis of and Conservatisms Inherent to the Equation Used to Estimate Leakage

The parallel plate model for crack flow has been applied by various researchers in the petroleum and water resources fields since the 1950's. A demonstration of the validity of the theory for laminar flow in both smooth- and rough-walled plates may be found, for example, in the work of Huitt[1], who showed that such flow obeys Darcy's law for low Reynolds numbers. This work was amplified and extended by Louis[3] who experimented on a wider range of surface roughness and flow rates, and produced a set of empirical equations for smooth- and rough-walled cracks under both turbulent and laminar flow.

Louis' equations for smooth-walled and laminar flow are the same as those used in deriving equation (7). His equation for rough walled cracks is a function of the relative roughness $K_r = E/2b$, where E is defined as the depth of surface roughness (measured peak to trough), and b is the nominal crack aperture. If the crack exhibits surface roughness, the smooth-walled flow rate for a given gradient is reduced by multiplying by the factor $1/(1 + 8.8\ K_r^{1.5})$. As an example, cracks with surface roughness equal to 20 percent of aperture, a value generally exceeded in concrete flexural cracks, would conduct approximately 22 percent less flow than smooth cracks. The calculated leakage determined herein is thus conservative since surface roughness effects were not considered.

Another factor which conservatively is not considered in the idealization to parallel plate flow is tortuosity, as it affects crack length. Flow rate for a given gradient is inversely proportional to crack length through the wall, thus the effect of crack tortuosity is to increase the actual length of the flow path and decrease the flow rate. The assumption of laminar flow is also conservative because the flow rate varies directly with the change in gradient, whereas under turbulent conditions, the flow rate varies approximately with the square root of the gradient. From the above conditions, it can be concluded that the use of a laminar smooth-walled parallel plate flow model for cracks will tend to over estimate the true flow rate which would occur in non-ideal rough-walled, tortuous fractures which may, in fact, experience turbulent flow. Therefore, the use of equation (7) will yield conservative estimates of flow through cracks in the reinforced concrete walls.

4.2 Case Studies

The results of the analysis of the distribution of cracks and maximum crack openings are shown on Figures 4.2, 4.3 and 4.4. Specifically, Figure 4.2 shows the maximum crack pattern in the most critical wall due to water and seismic induced loadings for the condition of the concrete enclosure containing 500,000 gallons of water, and Figure 4.3 shows the corresponding crack pattern for 280,000 gallons of water in the

enclosure. The crack pattern for the other three walls was calculated to be as shown on Figure 4.4 for the 500,000 gallon case. Equation (7) of Table 4.1 was used to estimate leakage through the cracks. All cracks were assumed to have a cross-sectional configuration defined by the maximum aperture at the inside or outside face of the wall as defined on Figure 4.2 and 4.3, and to have a uniform reduction over a length of about 18 inches to a minimum aperture of 0.001 inches. This minimum aperture is constant over the last six inches of wall. In the case where the aperture at the inside face of the wall was less than .001 inches, a constant aperture equal to the aperture at the inside face of the wall was assumed. Equivalent uniform apertures were calculated for each crack using the relationships shown on Table 4.2. Vertical cracks were characterized in a conservative manner by three equivalent horizontal cracks at elevations 16.7, 11, and 6.2 ft. as described above and on Fig. 4.1.

The most severe crack occurs at the base of the wall where imposed seismic and hydrodynamic moments are the greatest. Figure 4.5 shows the most conservative interpretation of this crack considering the maximum apertures at the inside and outside faces of the wall simultaneously. The maximum crack aperture of 0.039 inches is shown on the inside face of the wall, and it decreases uniformly to a minimum aperture of .023 inches at the outside face of the wall. Because of the geometry of the shear key, a minimum aperture of .008 and 0.007 inches occur at segments BC and ED of the crack as shown in Figure 4.5.

In this respect it is noted that the effect of the outward hydrostatic loading imposed by the spilled total contents of the tank is to enlarge the crack aperture on the inside face of the walls and to reduce the aperture on the outside face. For this analysis a conservative combination of apertures was selected wherein the maximum hydrostatic loadings were considered in calculating the enlarged inside aperture but were disregarded in reducing the outside aperture.

The maximum crack apertures shown on Figures 4.3, 4.4, and 4.5 were developed from the governing crack analysis described above. The minimum aperture of .001 inches for all cracks (except for the foregoing conserrvative interpretation for the base crack in the wall shown on Figures 4.2 and 4.5) was developed considering the 250 to 500 psi range of normal compressive stress calculated at the various sections from the flexural moment obtained under the sustained hydrostatic load as presented in Appendix A. The stress is relevant to evaluate the minimum crack aperture at locations where the linear behavior prevails and the flexural compression zone may experience prior cracking due to moment reversal caused by the lateral seismic inertial load from the walls. The effect of this normal compressive stress is to induce contact and closure of the crack, which in turn tends to decrease the flow rate. The effect has been evaluated from laboratory tests performed on cracks in various natural materials. Work performed by Iwai[2] on basalt, granite and marble is used as described in Appendix C to develop the effect of stress on crack aperture as shown on Figure 4.6. Though no data are available for concrete, the granite and marble data approximate concrete as the concrete is composed of granitic aggregate in a limestone matrix similar to marble. It is expected that variations in this data would be minimal for concrete and the leakage results would be well bounded by the conservative assumption of the lower crack dimension in Figure 4.5. An aperture of .001 inches represents a conservative interpretation of the referenced test data.

In the case where leakage was calculated across the specific crack shown in Figure 4.5, the presence of the water stop was neglected as were the waterproofing compound between the inside wall face and the new top mat slab. The presence of the new concrete mat itself, which will be placed to improve seismic anchorage of the base of the tank, was also neglected for conservatism.

Specific cases included in the analyses were:

1. the maximum crack pattern with no leakage through the bottom crack due to the presence of the water stop for an initial volume of 500,000 gallons of water (Figure 4.2);

2. the same as case 1 but conservatively neglecting the water stop throughout the total crack length and assuming leakage through the bottom crack on the vertical wall characterized on Figure 4.2 excluding the cracks identified by asterisks. These crack widths become .001 inches upon consideration of closure due to hydrostatic loading. Case 5 describes the conservative case where hydrostatic closure was neglected.

3. the maximum crack pattern with no leakage through the bottom crack due to the presence of the water stop for an initial volume of 280,000 gallons of water (Figure 4.3);

4. the same as case 3 but neglecting the water stop and assuming leakage through the bottom crack;

5. the same as case 1 but neglecting the water stop in the critical wall and assuming the most critical combination of apertures as indicated by the table in Figure 4.5; and

6. additional leakage obtained from permeable flow through sound concrete.

For all the above cases except cases 5 and 6, the crack pattern in the most critical wall was conservatively assumed to occur in all four walls by multiplying the leakage for the most critical wall (Figures 4.2 and 4.3) by a factor of 4. Under case 6 the seepage due to the permeability of uncracked concrete was considered. The permeability coefficient was determined per references (5) and (6) based on the maximum aggregate size of 1-1/2 inch and the favorably low water/cement ratio of 0.57 corresponding to the concrete mix (with 10% pozzolan) used in the enclosure structure. The total surface area of the walls and base mat was considered, and conservatively, all were subject to the maximum head of 22.5 feet of water.

At the request of the NRC staff a seventh case was also evaluated to determine how large a localized aperture at the bottom of the wall would have to be to discharge the 260,000 gallons of excess water not required for cooling over the 24 hour period upon starting with the 500,000 gallon initial volume case. The maximum length of opening was assumed to be equal to the reinforcing bar spacing (1-ft) because the reinforcing steel would restrain a localized opening due to its tensile capacity. With this restraint in effect, the minimum aperture of the bottom crack was back calculated such that 260,000 gallons of water would be discharged in 24 hours. In the interest of conservatism all calculations were made assuming no reductions in head due to intentional drawdown for cooling water.

4.3 Results of Analyses

The calculated leakage for cases 1 and 2 defined above was less than 1500 and 3000 gallons in 24 hours, respectively. The corresponding leakage for cases 3 and 4 was less than 150 gallons for either case. For case 5, less than 40,000 gallons of leakage in 24 hours is calculated. A summary of the results of these first five cases is presented on Table 4.3 along with a schematic description of the geometry of the base crack for each case. For case 6 the calculated leakage is insignificant amounting to 1.5 gallons over the 24 hour period. For the localized 1/2- to 1-foot long crack at the bottom of the wall the average aperture through the wall required to casue 260,000 gallons of leakage in 24 hours was calculated to be about .05 to .08 inches. This is almost two orders of magnitude greater than the conservative .001-inch minimum aperture of most of the crack and about one order of magnitude greater than the minimum aperture of the base crack (where the water stop is effective) of the most critical wall characterized on Figure 4.2. If the reduction in head resulting from the intentional drawdown of the water in the room is incorporated in this last extreme analysis of a localized opening, an additional 80,000 to 100,000 gallons of water would remain in the room at the end of 24 hours (i.e., 80,000 to 100,000 gallons less leakage from cracks would occur).

In summary, the Applicant estimates that less than 1500 gallons of water would leak through the Condensate Storage Building walls in 24 hours under the worst loading conditions (i.e., high water level due to 500,000 gallons of water with DBE loading0. By neglecting the effectiveness of the water stop throughout the length of the base crack in the most critical wall the resulting leakage would still be less than 3000 gallons which is less than 2% of the excess 260,000 gallons of water available for cooling for that period.

Assuming the most critical combination of apertures as indicated in the table on Figure 4.5 (a condition that is not credible because the maximum aperture on the outside face neglects the hydrostatic head but represents an extreme limiting calculation) leakage would be less than 40,000 gallons in 24 hours. Further, the Applicant calculates that a local aperture of a crack restrained in length by the reinforcing bar spacing could be almost two orders of magnitude greater than the conservative .001 inch opening at the outside face of the wall and still leave almost 100,000 gallons of excess water in the room after 24 hours.

REFERENCES

(1) Huitt, J. L., "Fluid flow in simulated fractures," AICHE Journal, v. 2, p. 259, 1956.

(2) Iwai, K., "Fundamental studies of fluid flow through a single fracture," Ph. D. thesis, University of California, Berkeley, 208 p., 1976.

(3) Louis, C., "Stromungsvorgange in Kluftigen Medien and ihre Wirkung auf die Standischerheit von Bauwerken und Boschungen im Fells," Dissertation Universitat (TH) Karsruhe, 1967. Also published in English as: "A study of groundwater flow in jointed rock and its influence on the stability of rock masses," Imperial College Rock Mechanics Research Report No. 10, September 1969.

(4) Wilson, C. R., and Witherspoon, P. A., "An investigation of laminar flow in fractured porous rocks," Department of Civil Enginering Publication 70-6, University of California, Berkeley, 1970.

(5) Concrete Manual. A water resources technical publication, U.S. Department of the Interior, Bureau of Reclamation. Eighth Edition, 1975; Figure 17.

(6) Mass Concrete for Dams and Other Massive Structures, reported by ACI Committee 207; Table 3.5.1.

Table 4.1 SUMMARY DEVIATION OF LEAKAGE EQUATIONS

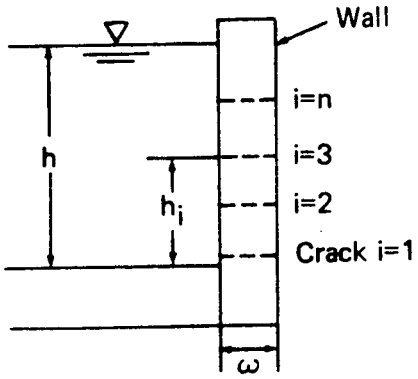

A = Area of Room
b_i = Aperture of Crack i
L_i = Length of Crack i
ρ = Mass Density of Water
g = Acceleration due to Gravity
μ = Viscosity of Water
ω = Width of Wall
h = Height of Water in Room

line no

FLOW RATE: $Q = K \; i \; A'$ (1)

K: Hydraulic Conductivity; i: Gradient; A': Flow Area

USING THE PARALLEL PLATE MODEL (HUITT 1956)

$$A\frac{dh}{dt} = \left(\frac{b^2\rho g}{12\mu}\right)\left(\frac{h-h_i}{\omega}\right)\left(bL\right) \quad (2)$$

FOR n CRACKS:

$$A\frac{dh}{dt} = -\left\{\left[\sum_{i=1}^{n}\frac{\rho g}{\mu}\frac{b_i^3}{12}\frac{L_i}{\omega}\right]h(t) - \sum_{i=1}^{n}\frac{\rho g}{\mu}\frac{b_i^3}{12}\frac{L_i}{\omega}h_i\right\} \quad (3)$$

ISOLATING CONSTANTS

$$\text{let } C_i = \frac{\rho g}{\mu}\frac{b_i^3}{12}\frac{L_i}{\omega} \text{ and } C_n = \sum_{i=1}^{n} C_i \quad (4)$$

$$\text{also } M_i = C_i h_i \text{ and } M_n = \sum_{i=1}^{n} M_i \quad (5)$$

AND SIMPLIFYING:

$$A\frac{dh}{dt} = -\left[C_n h - M_n\right] \quad (6)$$

UPON INTEGRATION:

$$-\frac{A}{C_n}\ln\left[\frac{C_n h_t - M_n}{C_n h_o - M_n}\right] = t - t_o \quad (7)$$

Table 4.2 CALCULATION OF EQUIVALENT APERTURES

Wedge shaped cracks: $b_1 > b_2$

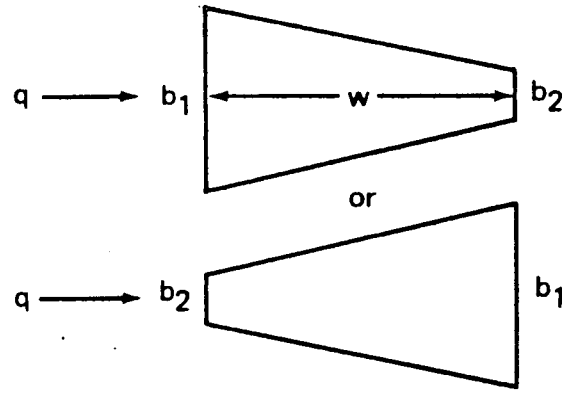

$$b^3_{eff} = \frac{2b_1^2 b_2^2}{b_1 + b_2}$$

(Appendix B, Reference B-1)

Cracks in series:

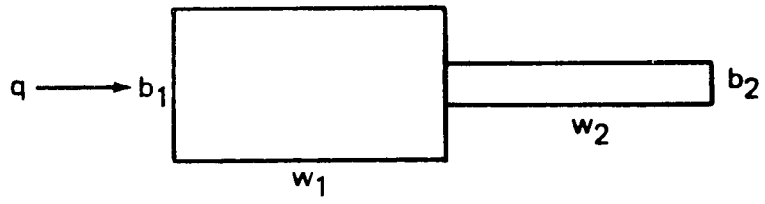

$$b^3_{eff} = \frac{w_1 + w_2}{\frac{w_1}{b_1^3} + \frac{w_2}{b_2^3}}$$

(Appendix B, Reference B-1)

Cracks in parallel:

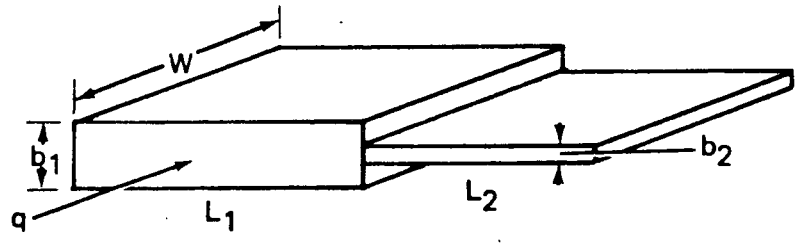

$$b^3_{eff} = \frac{L_1 b_1^3 + L_2 b_2^3}{L_1 + L_2}$$

(Appendix B)

Table 4.3 SUMMARY OF RESULTS OF ANALYSES FOR CASES 1 THROUGH 5

CASE	DESCRIPTION	RESULTING ESTIMATED LEAKAGE	GEOMETRY OF BASE CRACK *
1	Crack pattern shown on Figure 4.2 on all walls with no leakage along the dashed crack where the water stop is effective. (Actual crack configuration for 500,000 gallon tank volume)	<1,500 gallons in 24 hours	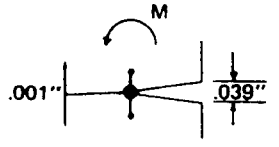
2	Same as Case 1 except that leakage is assumed from the dashed crack on Figure 4.2 (neglect water stop) on all walls. This is conservative in that the water stop is neglected and the largest crack from the wall with the longest span is assumed for all walls.	<3,000 gallons in 24 hours	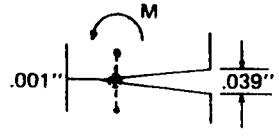
3	Crack pattern shown on Figure 4.3 on all walls with no leakage along the dashed crack where the water stop is effective. (Actual crack configuration for 280,000 gallon tank volume.)	<150 gallons in 24 hours	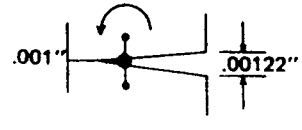
4	Same as Case 3 except the dashed crack on Figure 4.3 leaks (neglect water stop) on all walls.	<150 gallons in 24 hours	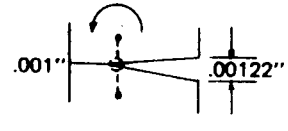
5	Same as Case 1 except assume the dashed crack on Figure 4.2 on one wall exhibits the most conservative combination of apertures as shown on Figure 4.5.	~40,000 gallons in 24 hours	See Figure 4.5

*Solid water stop indicates that it is effective to stop leakage. Dashed water stop indicates that it was neglected in leakage calculation.

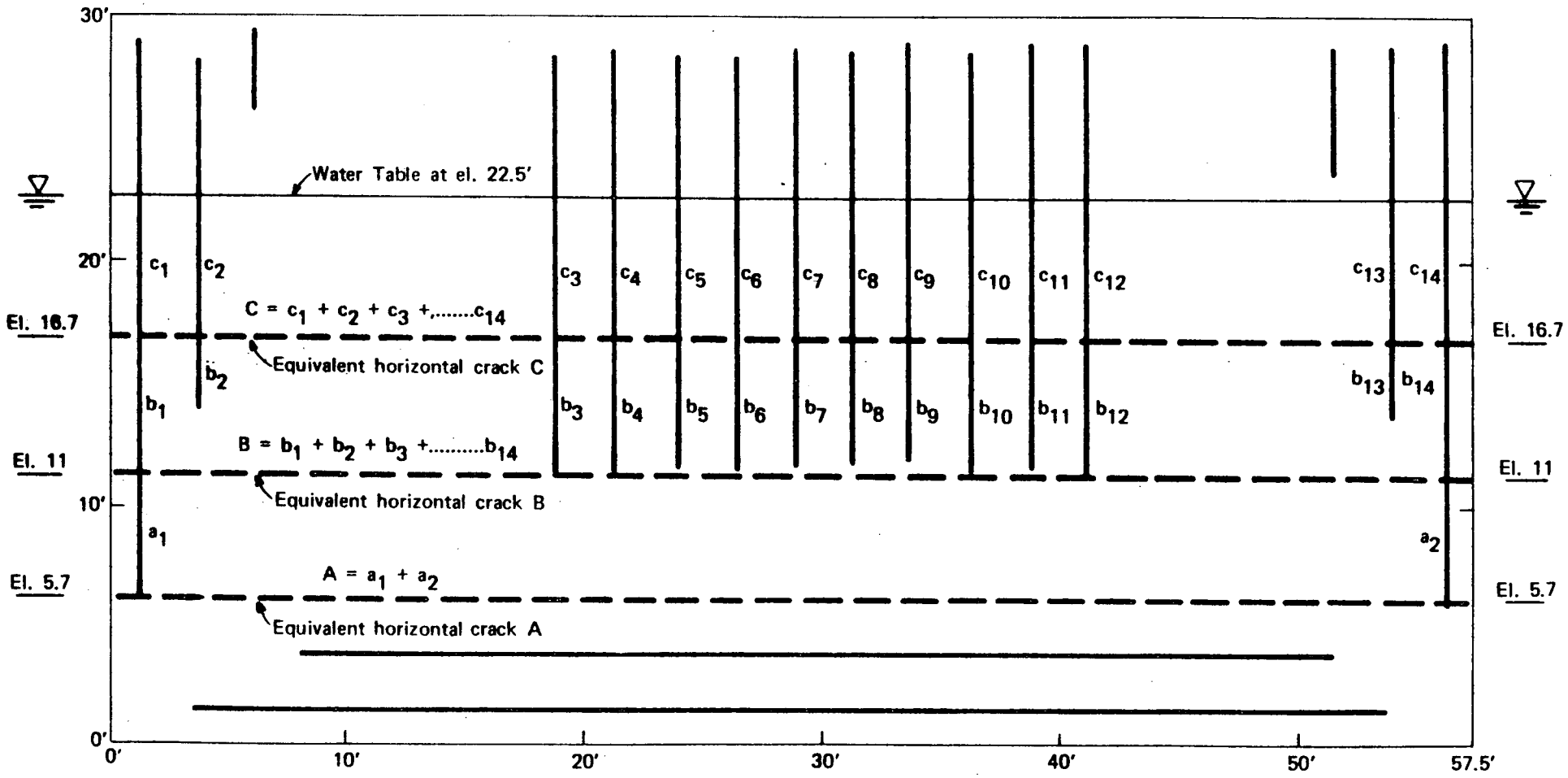

Figure 4.1 EXAMPLE OF MODELING VERTICAL CRACKS BY EQUIVALENT HORIZONTAL CRACKS

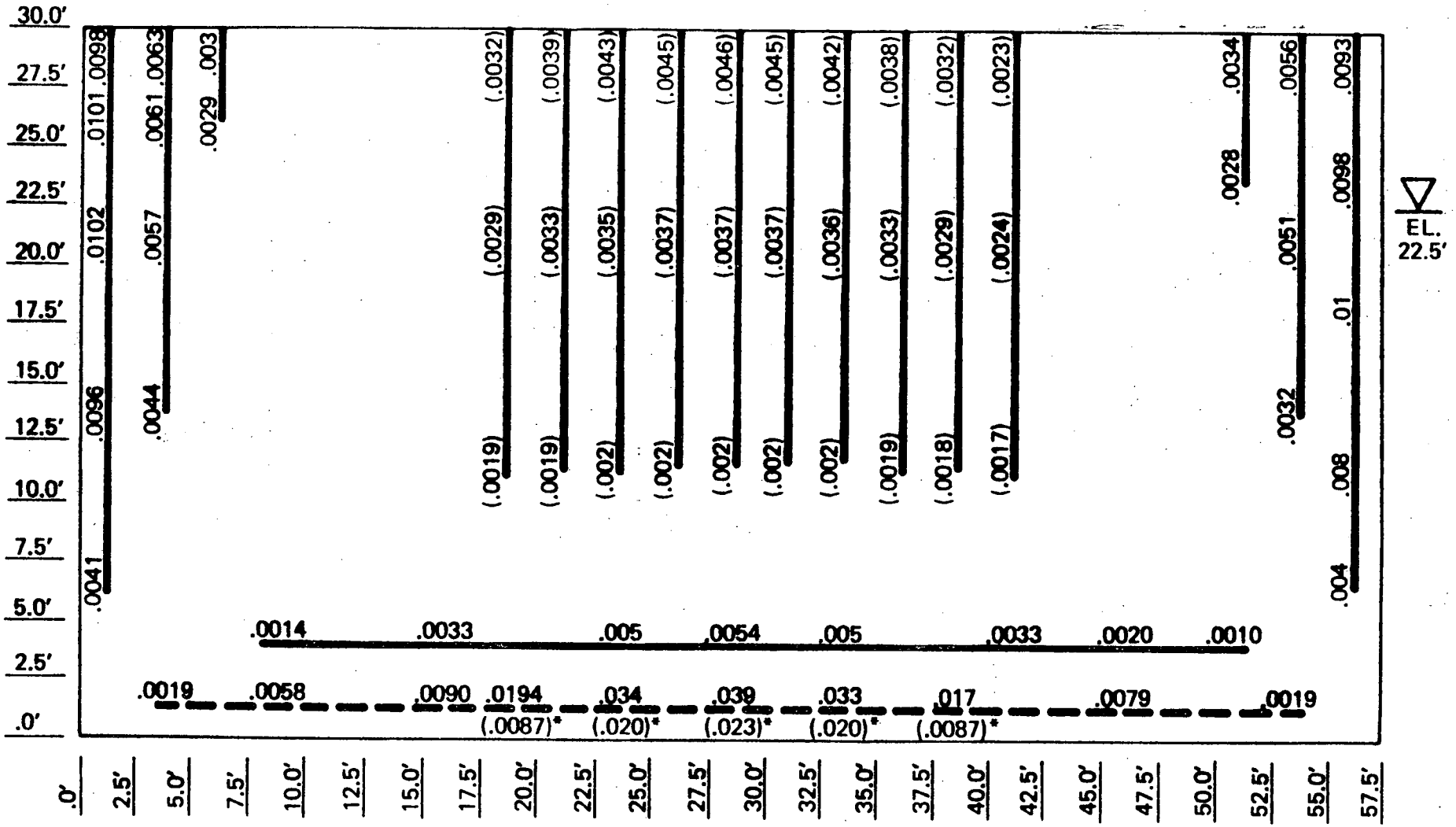

Figure 4.2 CONDENSATE STORAGE TANK AREA WALL–1
DIAGRAM SHOWING CRACK APERTURES IN INCHES

Crack apertures shown relate to maximum aperture on inside wall face.
Crack apertures shown in parenthesis indicate maximum aperture on outside wall face.
Bottom crack shown by a dashed line contains the water stop.
* These apertures occur only with no hydrostatic pressures on the wall; therefore the combination of apertures shown is the most conservative combination.

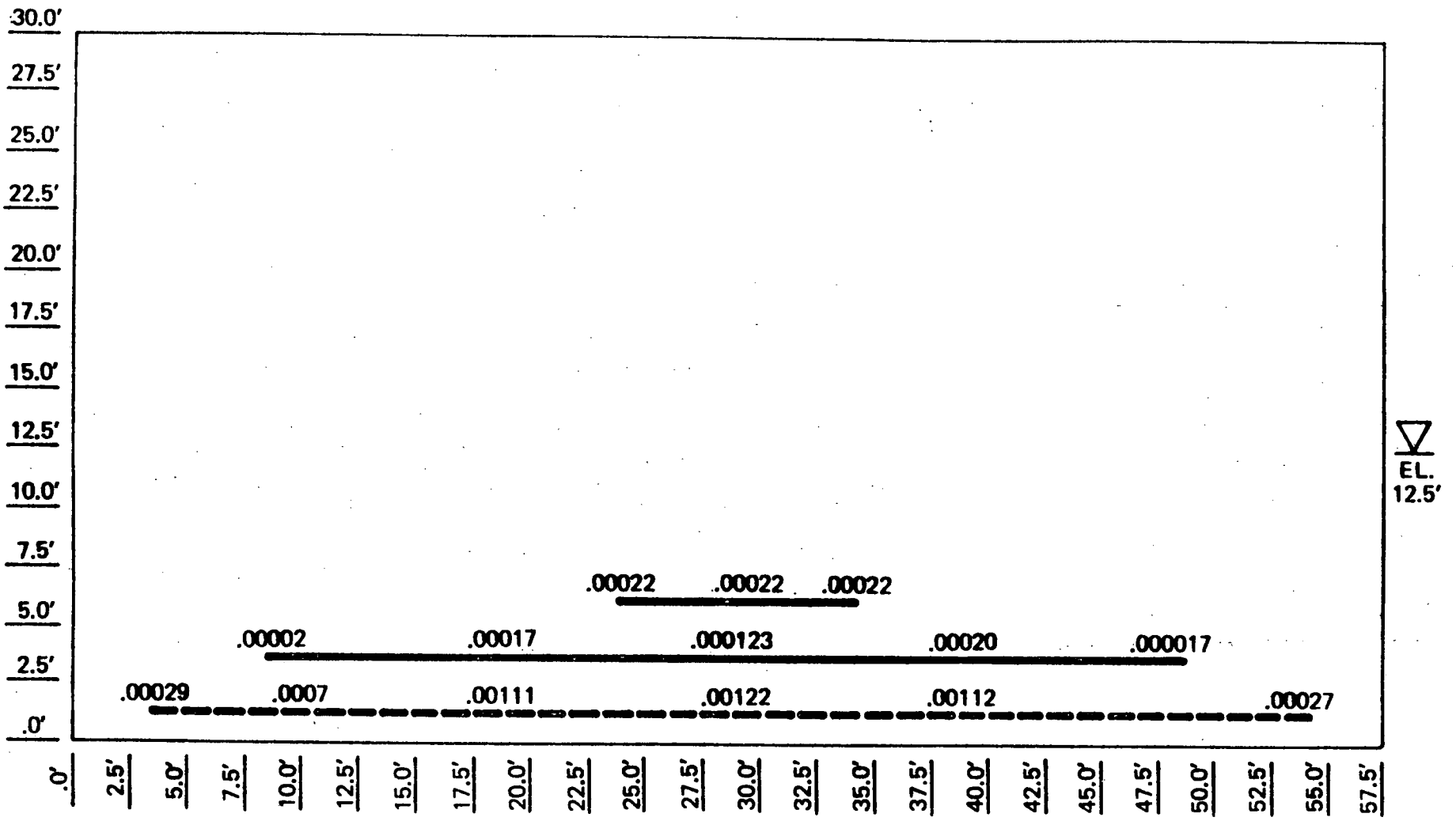

Figure 4.3 CONDENSATE STORAGE TANK AREA WALL–1
DIAGRAM SHOWING CRACK APERTURES IN INCHES

Crack aperture shown relate to maximum aperture on inside wall face.
Bottom crack shown by dashed line contains the water stop.

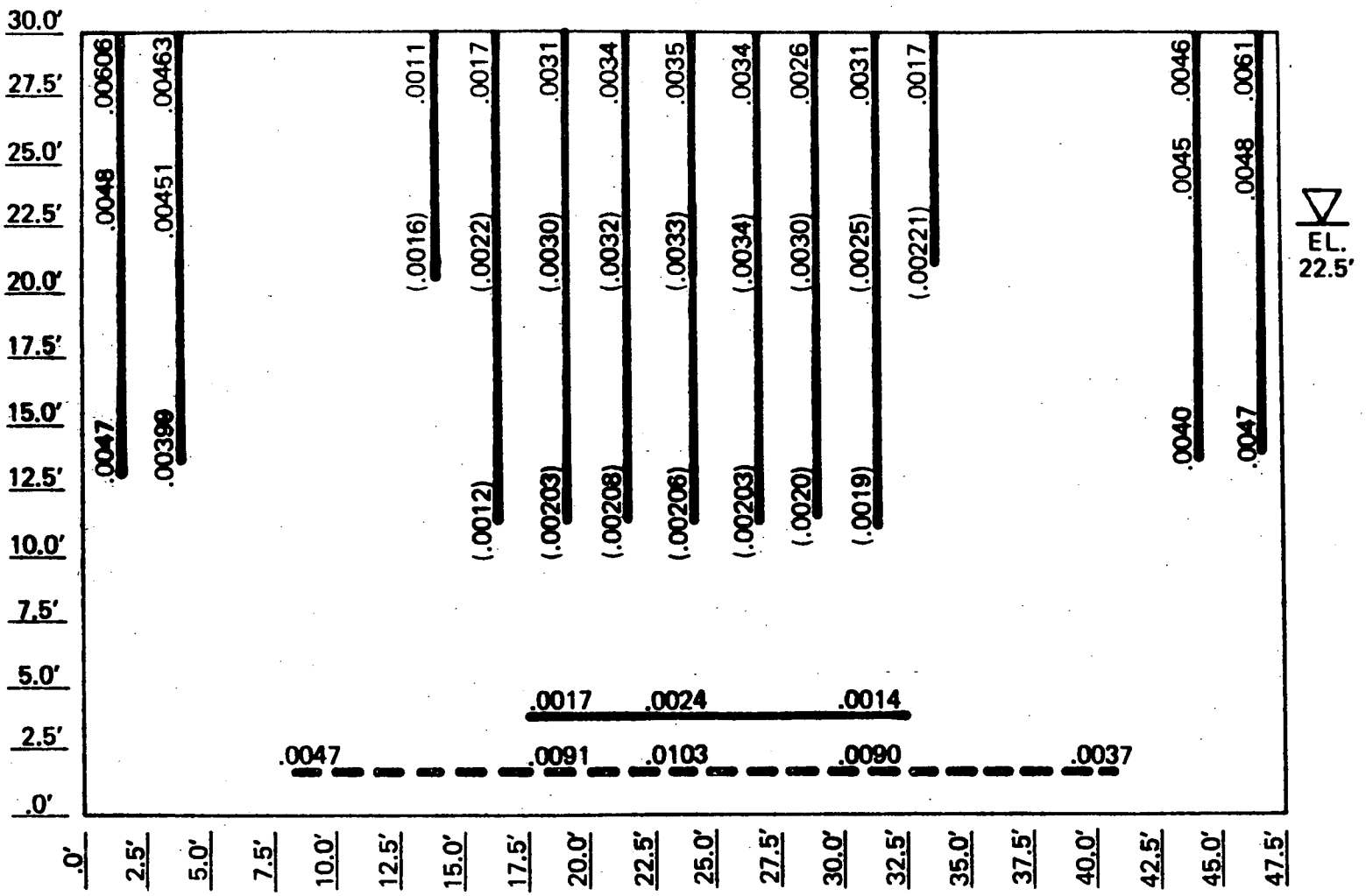

Figure 4.4 CONDENSATE STORAGE TANK AREA WALL–4
DIAGRAM SHOWING CRACK APERTURES IN INCHES

Crack apertures shown relate to maximum aperture on inside wall face.
Crack apertures shown in parenthesis indicate maximum aperture on outside wall face.
Bottom crack shown by a dashed line contains the water stop.

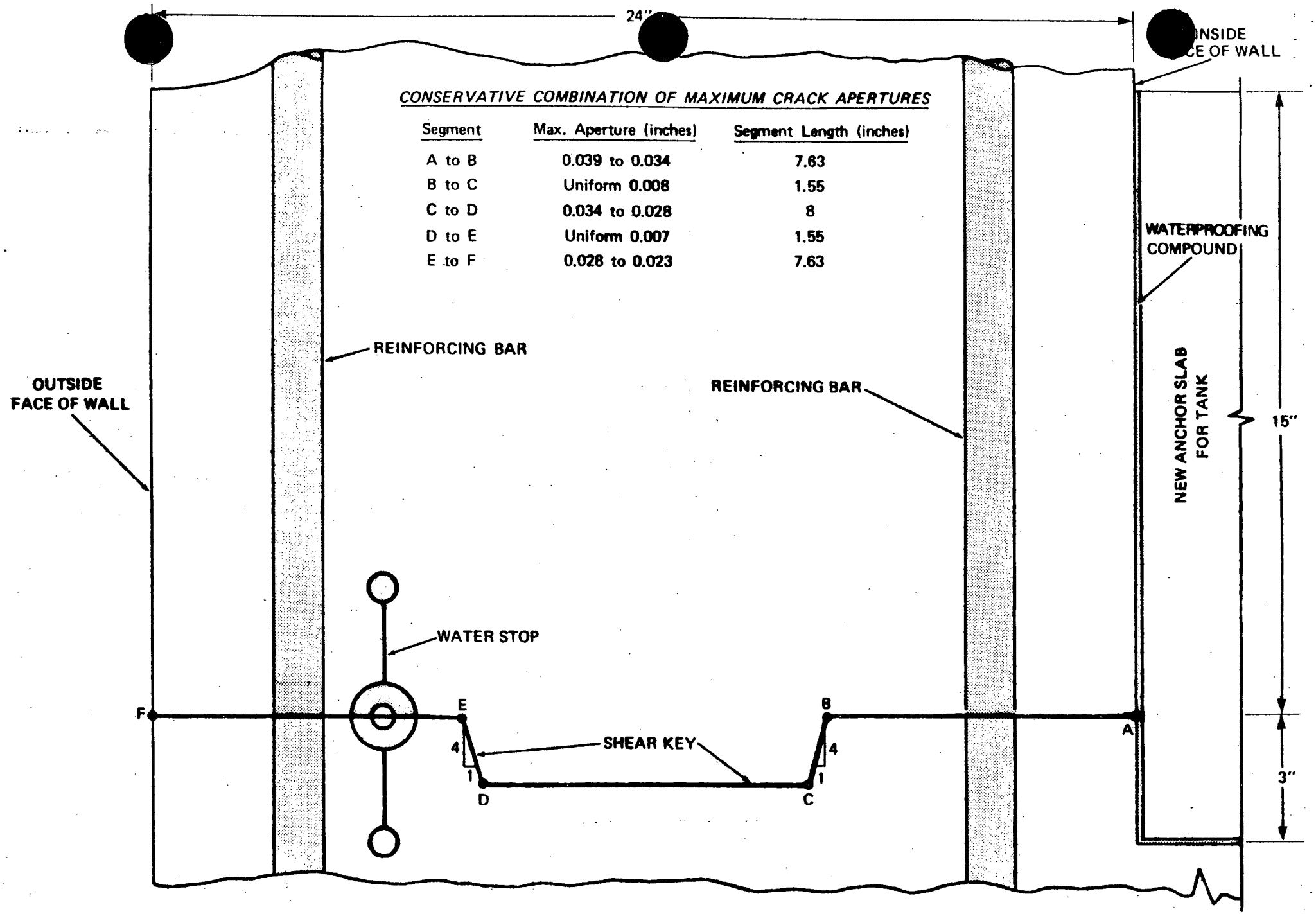

Figure 4.5 SECTION THROUGH BASE OF WALL

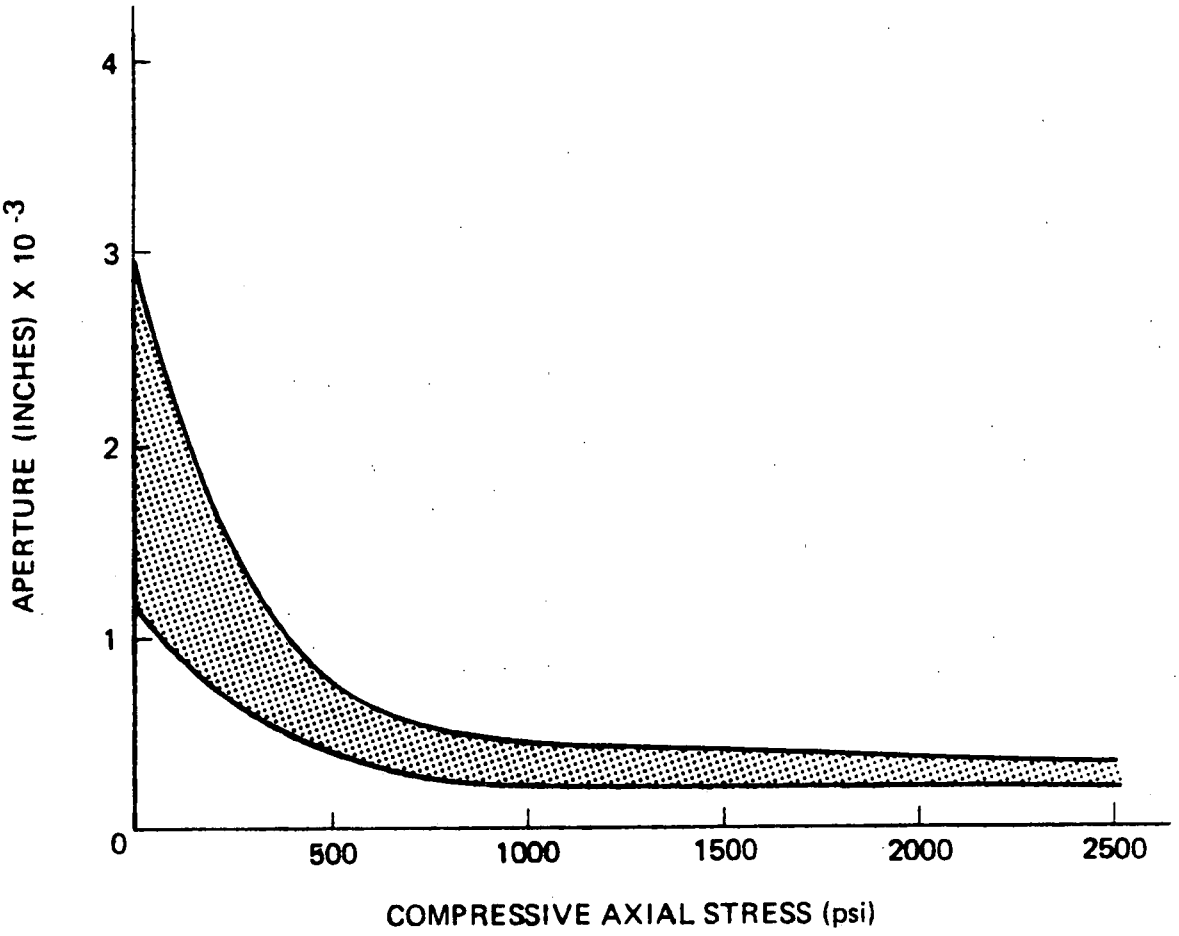

Figure 4.6 EFFECT OF COMPRESSIVE STRESS ON APERTURE

Appendix B. Backup for Table 4.2

The equation for wedge shape fracture is discussed on pages 60 and 61 of the attached Wilson and Witherspoon (1970) paper attached as reference B-1 which references experiemental verification by Lomize (1951).

The equation for cracks in series are developed theoretically in Wilson and Witherspoon (1970) on pages 57 through 60 and checked for consistency with Lomize (1951) experimental work on wedge shaped cracks. (Note that equation II-28 is identical to the appropriate equation in Table 4.2 except that crack length is designated by "l" in equation II-28 and by "W" in Table 4.2).

The equation for cracks in parallel is simply a weighted average on b^3 for which there is ample experimental verification that flow is proportional to b^3 as discussed in Witherspoon et al. (October 1979) attached.

Reference B-1
Pages 55 through 62, 165 and 168

AN INVESTIGATION OF LAMINAR FLOW IN FRACTURED POROUS ROCKS

by

Charles R. Wilson

and

Paul A. Witherspoon

Department of Civil Engineering
University of California
Berkeley

November 1970

$$\frac{\partial J}{\partial \phi_m} = \frac{1}{2D}\left[\left(K_{xx}b_m b_i + K_{xz}(c_m b_i + b_m c_i) + K_{zz}c_m c_i\right)\phi_i + \left(K_{xx}b_m b_j + K_{xz}(c_m b_j + b_m c_j) + K_{zz}c_m c_j\right)\phi_j + \left(K_{xx}b_m b_m + K_{xz}(c_m b_m + b_m c_m) + K_{zz}c_m c_m\right)\phi_m\right]$$

These solutions are valid only for elements whose nodes both i and j lie on a boundary, and node m does not lie on a boundary. For an element with only one node on the boundary, the integration along the length of the boundary is zero, the velocity term drops out, and the standard internal equation results. For nodes along boundaries of zero flow, V will be zero and the equations reduce to the standard internal equation. A copy of the finite element computer program produced from these theoretical considerations is presented in Appendix A.

2. Verification and Use of the Triangular Element Program

This program was verified by creating several simple problems which could be checked by hand. First, flow in a straight parallel-wall fracture was calculated, and the results were in good agreement with hand calculations. Next, a system with one fracture sloping upward at +4.5°, and a second fracture intersecting near the midpoint and branching down at -9.0° was checked (Fig. II-10).

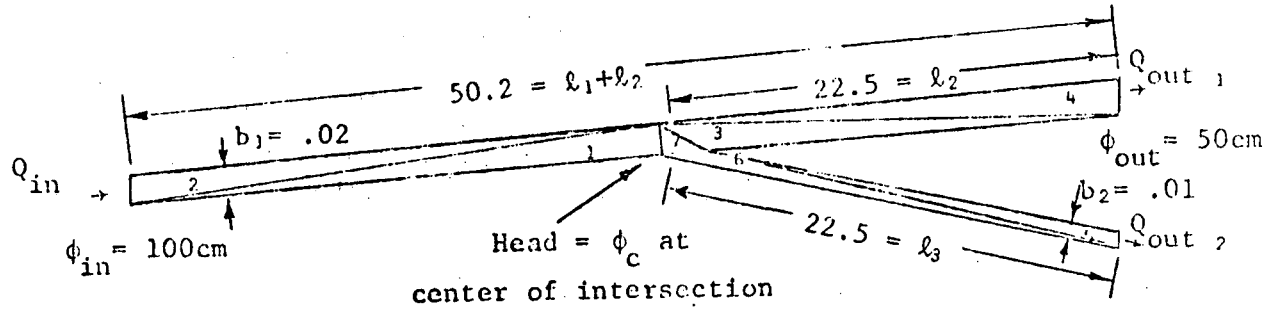

Fig. II-10: Plan for second check of computer program. Elements are numbered 1 to 7. Lengths and heads ϕ in cm units.

The hand solution is based on continuity, assuming that $Q_{in} = Q_{out\ 1} + Q_{out\ 2}$. Solving for the head at the intersection:

$$\phi_c = \frac{\frac{\phi_{in}K_1A_1}{\ell_1} + \frac{\phi_{out}K_1A_1}{\ell_2} + \frac{\phi_{out}K_2A_2}{\ell_3}}{\frac{K_1A_1}{\ell_1} + \frac{K_1A_1}{\ell_2} + \frac{K_2A_2}{\ell_3}} = 71.2 \text{ cm}$$

where:

$$K_i = \frac{b_i^2\gamma}{12\mu} \quad \text{and} \quad A_i = b_i \cdot 1$$

Thus:

$$Q_{in} = 5.90 \times 10^{-2} \text{ cm}^3/\text{sec}$$
$$Q_{out\ 1} = 5.32 \times 10^{-2} \text{ cm}^3/\text{sec}$$
$$Q_{out\ 2} = 0.66 \times 10^{-2} \text{ cm}^3/\text{sec}$$

The computer, using the finite element method, calculated the following values which compare quite well with the above results:

$$Q_{in} = 5.88 \times 10^{-2} \text{ cm}^3/\text{sec}$$
$$Q_{out\ 1} = 5.24 \times 10^{-2} \text{ cm}^3/\text{sec}$$
$$Q_{out\ 2} = 0.64 \times 10^{-2} \text{ cm}^3/\text{sec}$$
$$\phi_c = 71.6 \text{ cm}$$

The triangular finite element program can be effectively used to predict flow in fracture segments with an aperture that varies with length. Natural fractures have surfaces which are quite irregular in both the small details of the rough walls and the larger contortions of the channel. Laboratory studies performed on flow channels of varying shapes and roughnesses (Lomize[133], p. 88; Louis[135], p. 64; Huitt[100], p. 263) indicate that flow will be laminar in any of the conduits studied if the Reynolds Number

is less than about 200. Laminar flow in any conduit is always characterized by a linear relationship between velocity and gradient:

$$V = c \frac{\partial \phi}{\partial \ell}$$

where ℓ is measured along the path and the proportionality factor c, called the hydraulic conductivity, is a function of conduit geometry and fluid properties. For smooth wall parallel plate flow the hydraulic conductivity is equal to $b^2\gamma/12\mu$. Hence for a flow channel of any shape, if velocities are in the laminar range an aperture can be calculated for a smooth parallel plate conduit which will offer the same resistance to flow as the arbitrarily shaped channel. Therefore, in the laminar regime, any real fracture with its many contortions and wall asperities will behave in an overall sense, but not in terms of internal detail, as a parallel plate with a correctly chosen effective aperture b_{eff}.

A simple model of a fracture with varying aperture is presented in Fig. II-11 where three separate apertures are encountered along the length of the fracture. From continuity considerations similar to those used in the calculations accompanying Fig. II-10, the total flow was calculated by hand to be 0.0207 cm^3/sec. By assigning element apertures equal to the local width of the fracture, and setting the permeability ellipsoid orientation angle $\alpha = 0$ in all elements, the finite element result of 0.0201 cm^3/sec compares well with the hand calculated value.

From these same continuity considerations, the effective permeability for a fracture of three different apertures may be expressed as:

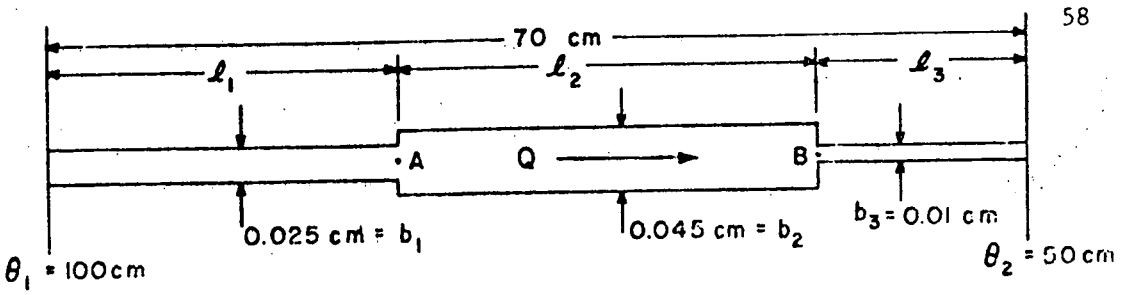

Fig. II-11. Fracture with irregular aperture.

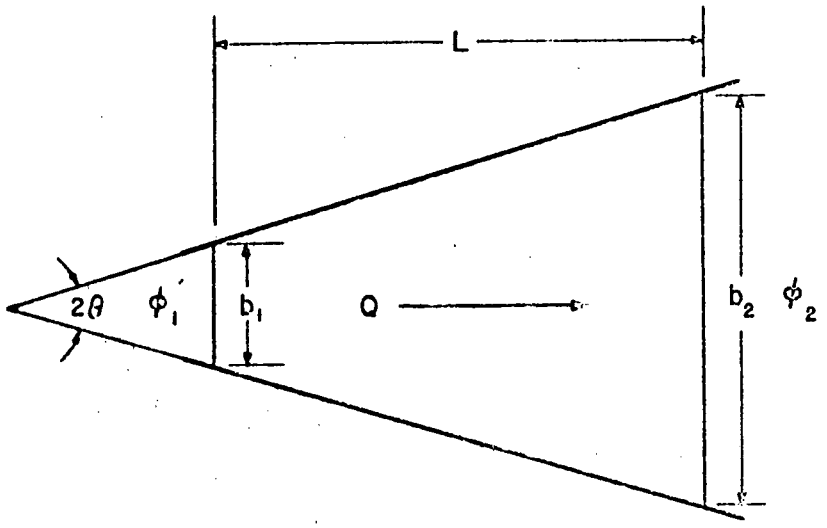

Fig. II-12. A wedge-shaped fracture.

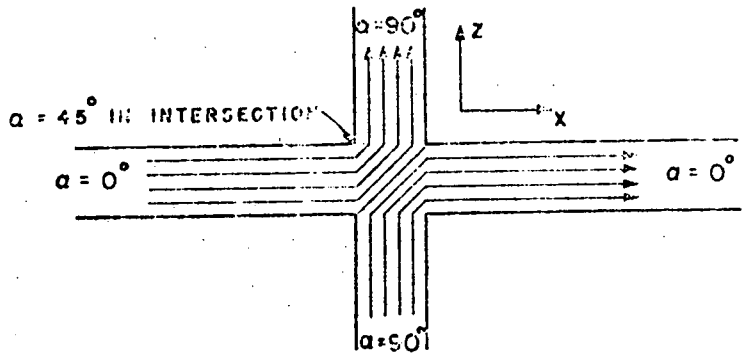

Fig. II-13. Idealized flow lines in intersecting fractures of identical aperture and flow. α gives orientation of K_x, in various regions.

$$b_{eff}^{3} = \frac{\ell_1 + \ell_2 + \ell_3}{\frac{\ell_1}{b_1^3} + \frac{\ell_2}{b_2^3} + \frac{\ell_3}{b_3^3}} \qquad \text{(II-28)}$$

whence $b_{eff} = 0.0161$ for the system of Fig. II-11. Calculating b_{eff} from the computer results yields:

$$b_{eff} = \left(\frac{12\mu Q_T L}{\gamma \Delta H}\right)^{\frac{1}{3}} = 0.0159 \text{ cm}$$

It is interesting to note that at point A in Fig. II-11, the head has dropped from 100 cm to 95.4 cm, and at point B it has further dropped to 94.5, leaving the remaining head of 44.5 cm to be lost in the short length of narrow channel. In this system 89% of the headloss occurs in only 21% of the length because of the smaller channel and the cubed relationship between aperture and flow volume.

It is evident from equation II-28 that for a flow channel of more than three apertures along its length, the effective aperture may be expressed as:

$$b_{eff}^{3} = \frac{\sum_{i=1}^{n} \ell_i}{\sum_{i=1}^{n} \frac{\ell_i}{b_i^3}} \qquad \text{(II-29)}$$

Or, if the aperture varies continuously along the length of the fracture, the effective aperture may be expressed as:

$$b_{eff}^{3} = \frac{\int_{o}^{L} d\ell}{\int_{o}^{L} \frac{d\ell}{b(\ell)^{3}}} \qquad \text{(II-30)}$$

The aperture b is now expressed as a function of path length ℓ along the fracture, where L is the total path length. This derivation assumes that locally the flow lines will be essentially horizontal and will not hold in those cases where apertures change abruptly along the length of the fracture.

As an example, the results of equation II-30 will be compared to a computer solution for the case of a wedge-shaped fracture (Fig. II-12). For this fracture, equation II-30 may be written:

$$b_{eff}^{3} = \frac{\int_{o}^{L} d\ell}{\int_{o}^{L} \frac{d\ell}{(m\ell + c)^{3}}}$$

where if 2θ is the angle of opening, then $m = 2 \tan \theta$, $c = b_1$ = aperture at smaller end, and $mL + c = b_2$ = aperture at larger end. The solution to this equation is:

$$b_{eff}^{3} = \frac{2mLb_1^{2}b_2^{2}}{b_2^{2} - b_1^{2}} = \frac{2b_1^{2}b_2^{2}}{b_1 + b_2} \qquad \text{(II-31)}$$

For example, if $b_1 = 0.205$ cm, $b_2 = 0.415$ cm, L = 20 cm, and $\theta = 0°18'$, then from equation II-31, $b_{eff} = 0.286$ cm. The computer, using 40 elements, obtained a value of $b_{eff} = 0.280$ cm. Even greater accuracy can be obtained

from the finite element method if more elements are used. Note that while equation II-31 is independent of L and θ, in reality θ must be rather small for flow to remain essentially horizontal.

A laboratory study of flow in wedge-shaped parallel plate conduits was performed by G. M. Lomize[133]. In one of Lomize's experiments, utilizing water in a conduit with the same dimensions as in the previous example, a flow rate of approximately 3 cm^3/sec per unit plate width was measured under a gradient of 0.02 cm/cm. From these results an effective aperture of b_{eff} = 0.27 cm is calculated.

This conduit has been modeled using 40 triangular elements. Assigning the same gradient of 0.02 cm/cm, and assuming unit density and a viscosity of 1 centipoise for the water in the test, the flow rate was calculated to be 3.6 cm^3/sec per unit width. This compares well with the experimental value, the discrepancies being due in a large part to slight roughnesses in the plate walls in Lomize's experiments (they cannot be ideally smooth as is assumed in the mathematical model). Also error occurs because the water temperature used in the calculations was assumed to be 70°F, which is probably not identical to the experimental conditions. No information was given by Lomize concerning temperature.

Since errors due to effects of wall roughness and temperature can be accounted for mathematically if these effects are known, in general the results should be as good as or better than those obtained above. This comparison with Lomize's experimental results indicates that fractures with gradually varying apertures can be accurately modeled using the two-dimensional finite element program.

Fracture intersections present a difficulty in the application of the triangular element program because hydraulic conductivity is not easily

defined in this space. The intersection belongs mutually to two separate fractures which may be of different aperture and hence different permeabilities, and at their juncture neither the magnitude nor the orientation of the permeability ellipsoid is defined.

The magnitude of the permeability which is mathematically identified with each triangular fracture element is related to an aperture assigned to that element. In an intersection or in other areas where the aperture is undefined the permeability is also undefined. Hence for elements in these regions it is necessary to arbitrarily select an "effective aperture" which will give a reasonable permeability value. By varying this effective aperture in intersection elements it is possible to introduce special headlosses into the model to account for interference effects which exist at intersections.

The magnitude of these effects was studied in the laboratory and the results are presented in Chapter III. They were found to be sufficiently small at low flow rates to be neglected, and it has been the practice in this paper to assign to intersection elements apertures equal to that of the larger fracture. However, the conductivity assigned to each fracture element is arbitrary and if it is desired, this model can be made to account for interference effects by assigning slightly smaller apertures to intersection elements.

The orientation of the permeability ellipsoid in each element is governed by the choice of angle α which determines specifically the orientation of the directional permeability K_x, within the permeability ellipsoid. Within a fracture segment it is clear that α should equal the fracture orientation, and that K_x, should equal $b^2\gamma/12\mu$, but within an intersection flow is undergoing abrupt changes in direction and also

90. Hartsock, J. H. and J. E. Warren, "The effect of horizontal fracturing on the well performance," J. Pet. Tech., p. 1050, 1961.

91. Heck, E. T., "Hydraulic fracturing in the light of geological conditions," Prod. Monthly, p. 12, September 1960.

92. Heitfeld, K. H., "Zur Frage der oberflachennahen Gebirgsauflockerung" (The question of surface loosening of rock masses), Proc. First Cong. of Int. Soc. Rock Mech., Lisbon, v. 1, p. 15, 1966.

93. Hobbs, D. W., "The formation of tension joints in sedimentary rocks: an explanation," Geol. Mag., v. 104, p. 550, 1967.

94. Hodgson, R. A., "Regional study of jointing in Comb Ridge, Navajo Mountain area, Arizona and Utah," Am. Assoc. Pet. Geol. Bull., v. 45, p. 1, 1961.

95. Holmes, C. D, "Tidal strain as a possible cause of microseisms and rock jointing," GSA Bull., v. 74, p. 1411, 1963.

96. Houpeurt A. and G. Manasterski, "Détermination de la perméabilité des roches à partir de la pression de déplacement d'un fluide homogène par un autre," Proc. 3rd World Petroleum Congress, v. 2, p. 460, 1951.

97. Hsu, C. C., "A simple solution for boundary layer flow of power law fluids past a semi-infinite flat plate," AIChE Jour., v. 15, p. 367, 1969.

98. Huang W., J. M. Robertson and M. B. McPherson, "Some analytical results for plane 90° bend flow," J. Hydraulics Div. ASCE, v. 93, no. 6, p. 169, 1967.

99. Hubbert, M. K. and D. G. Willis, "Mechanics of hydraulic fracturing," Trans AIME, v. 210, p. 153, 1957.

100. Huitt, J. L., "Fluid flow in simulated fractures," AIChE Jour., v. 2, p. 259, 1956.

101. Huskey, W. L. and P. B. Crawford, "Performance of petroleum reservoirs containing vertical fractures in the matrix," SPE Jour., p. 221, 1967.

102. Irmay, S., "Flow of liquid through cracked media," Bull. Res. Council of Israel, VSA, no. 1, p. 84, 1955.

103. Javandel, I. and P. A. Witherspoon, "Application of the finite element method to transient flow in porous media," Soc. Pet. Eng. Journal, v. 8, no. 3, p. 241, 1968.

129. Lewis, D. C. and R. H. Burgy, "Hydraulic characteristics of fractured and jointed rock," Groundwater, v. 2, no. 3, p. 4, July 1964.

130. Lewis, D. C., G. J. Kriz and R. H. Burgy, "Tracer dilution sampling technique to determine hydraulic conductivity of fractured rock," Water Resources Research, v. 2, p. 533, 1966.

131. Liakopoulos, A. C., "Darcy's coefficient of permeability as symmetric tensor of second rank," Bull. IASH, v. 10, no. 3, p. 41, 1965.

132. Limaye, D. G., "On the longevity of wells in the Deccan trap area," J. Inst. Engr., India, 1945.

133. Lomize, G., "Filtratsiia v treshchinovatykh porodakh," (Water flow in jointed rock) Gosenergoizdat, Moscow, 1951.

134. Londe, P., V. Gaston and R. Vormeringer, "Stability of rock slopes, a three dimensional study," J. Soil Mechanics and Foundation Div. ASCE, v. 95, no. 1, p. 235, 1969.

135. Louis, C., "Strömungsvorgänge in klüftigen Medien and ihre Wirkung auf die Standsicherheit von Bauwerken und Böschungen im Fels," Dissertation Universität (TH) Karlsruhe, 1967. Also published in English as: "A study of groundwater flow in jointed rock and its influence on the stability of rock masses," Imperial College Rock Mechanics Research Report No. 10, September 1969.

136. Lowe, D. K., B. B. McGlothlin and J. L. Huitt, "A computer study of horizontal fracture treatment design," J. Pet. Tech., p. 559, 1967.

137. Maksimovich, G. K., "Calculation of oil reserves in fissured reservoirs," Geologiya Nefti i Gaza, (English translation in Petroleum Geology) v. 2, no. 3, p. 258, 1958.

138. Maksimovich, G. A., "Basic types and the modulus of subsurface flow in karst regions," Proc. Acad. Scie USSR, Geol. Sci. Sec., v. 128, no. 5, p. 1039, (English translation p. 980) 1960.

139. Malaika, J., "Flow in non-circular conduits," J. Hydraulic Div. ASCE, v. 88, no. 6, p. 1, 1962.

140. Marcus, H., "Permeability of an anisotropic porous medium," JGR, v. 67, p. 5215, 1962.

141. Matthews, C. S. and D. G. Russell, "Pressure buildup and flow tests in wells," Chapter 10, Monograph no. 1, SPE, AIME, 1967.

Appendix C. Back Up for Figure 4.6

Figure 4.6 represents simply a cross plotting of normalized flow $Q/\Delta H$ versus axial stress σ_e (Figure 1 of Reference) and aperture 2b versus normalized flow graphs (Figure 5 of Reference). For granite these curves are presented on Figures 1 and 5 in Witherspoon et al., (October 1979) attached as reference C-1 and for marble and basalt they are presented on Figures 4.40 and 4.45 attached from Iwai's thesis and Figures 7 and 8 in Witherspoon et al., (October 1979). These figures are labeled C-1 through C-6 and are used to explain the cross plotting completed to develop Figure 4.6. Specifically, for granite a range of axial stress values was obtained from the data on Figure C-1 for a selected value of $Q/\Delta h$. The value of aperature corresponding to the same value of $Q/\Delta h$ was then obtained from the 2b vs. $Q/\Delta h$ graph at the top of Fig. C-2. The value of 2b (aperture) and range of σ_e (axial strss) was then plotted with aperature as the ordinate and compressive stress (axial stress) as the abscissa. Similar cross plotting was completed for marble using Figures C-3 and C-4 and for basalt using Figures C-5 and C-6. The range of values shown on Figure 4-6 approximately envelopes the data resulting from this cross plotting.

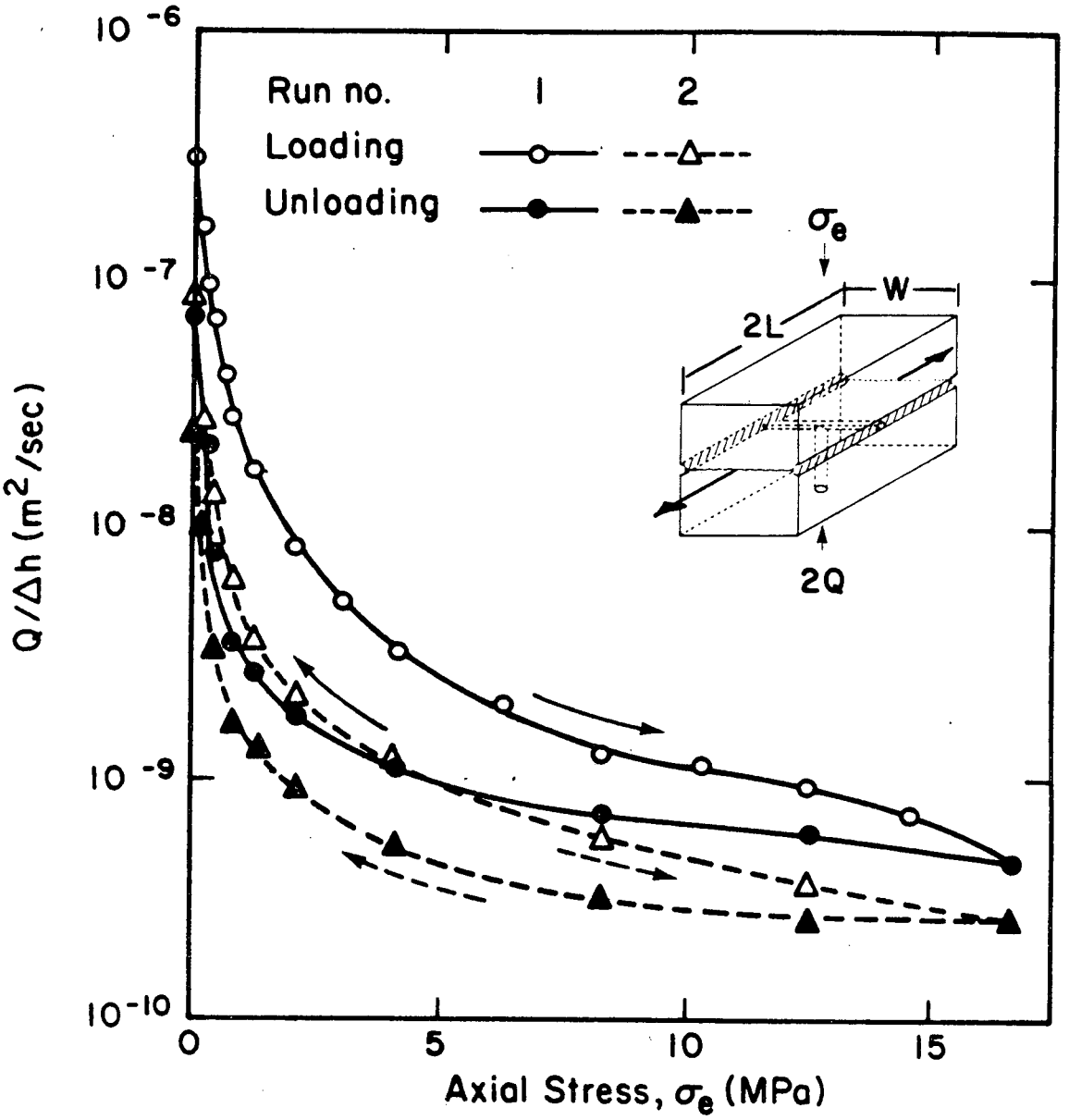

Fig. 1. Effect of cyclic loading on permeability of tension fracture in granite with straight flow (after Iwai, 1976).

Figure C-1 Granite

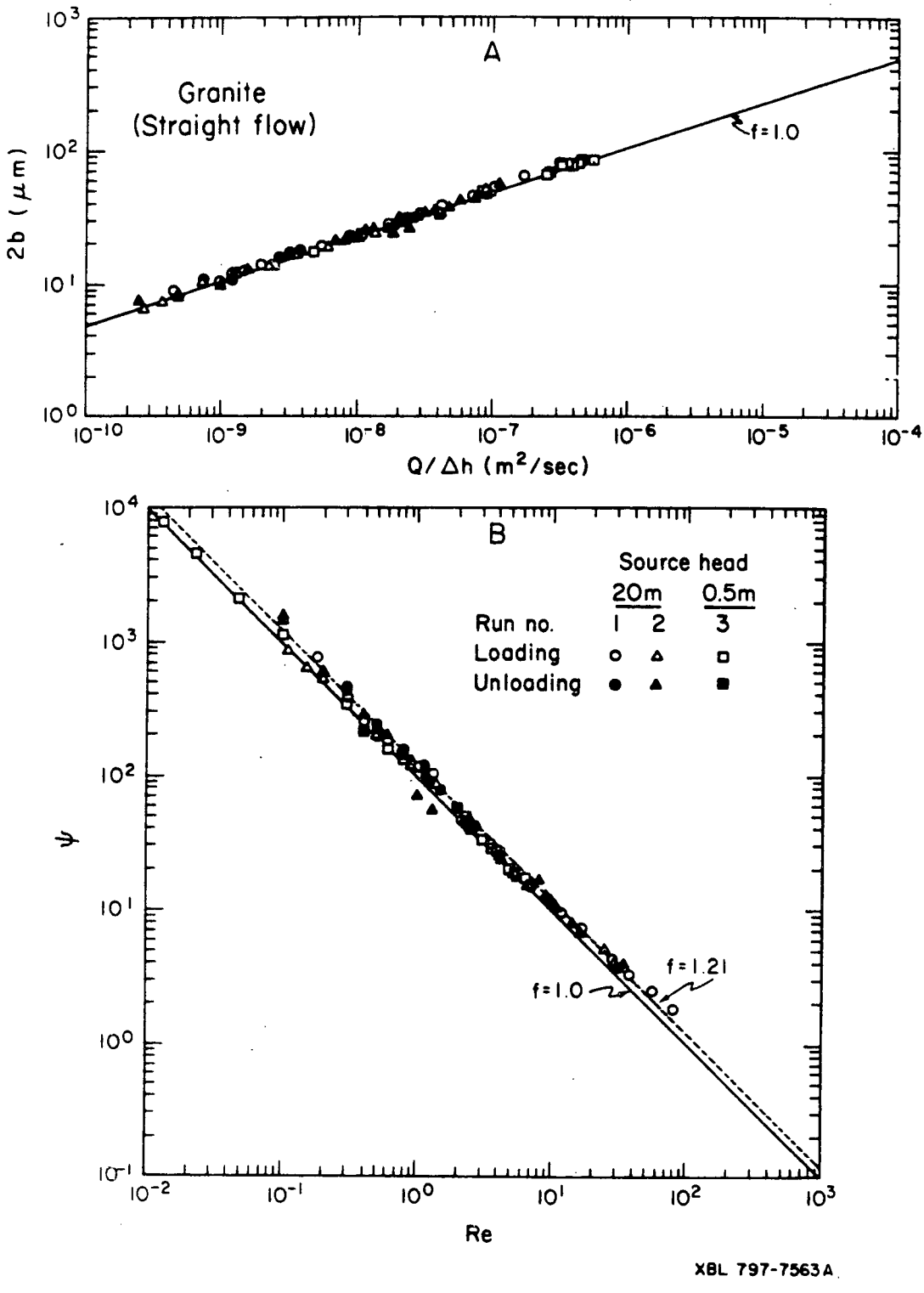

Fig. 5. Comparison of experiment for straight flow through tension fracture in granite with cubic law.

Figure C-2 Granite

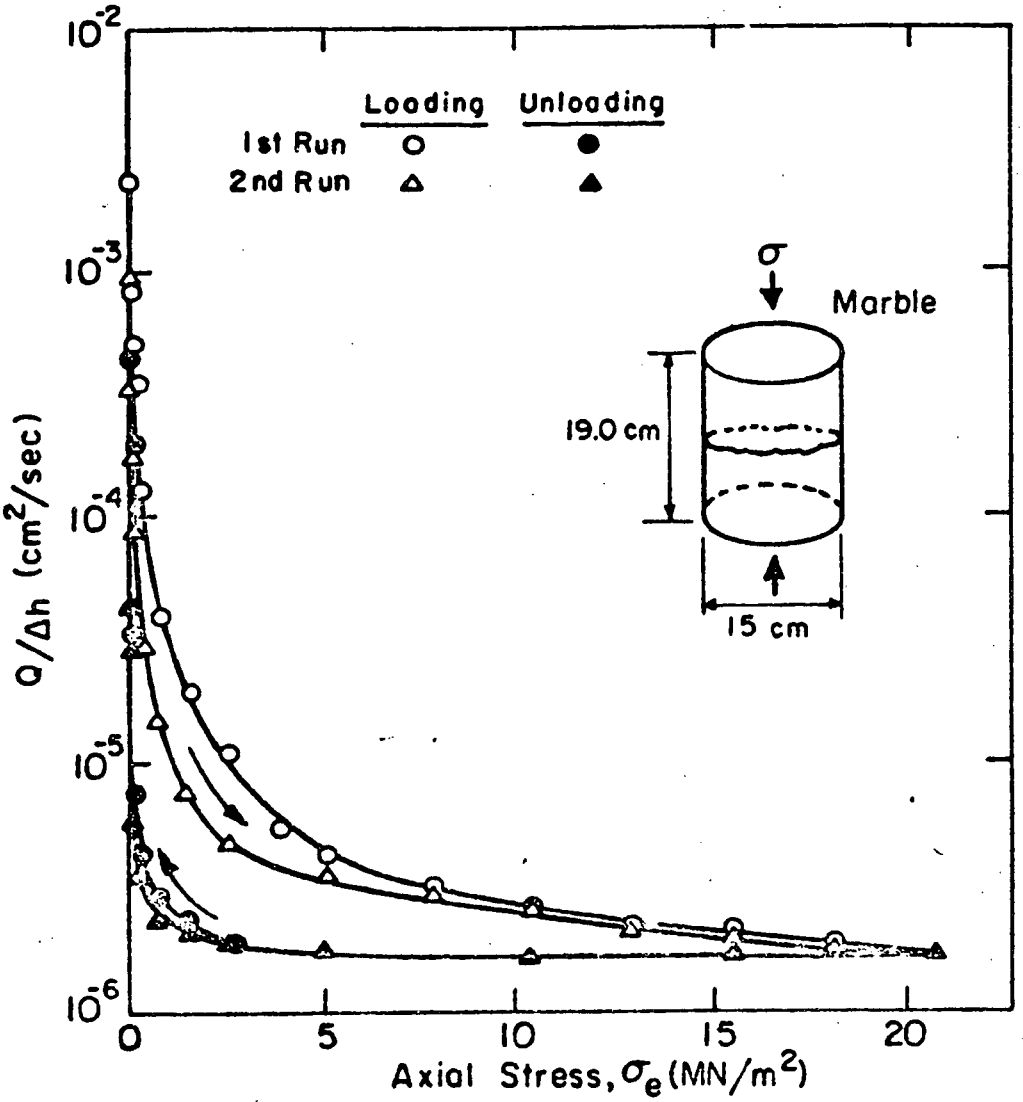

Fig. 4.45. Effect of cyclic loading on permeability of tension fracture in marble with radial flow.

Figure C-3 Marble

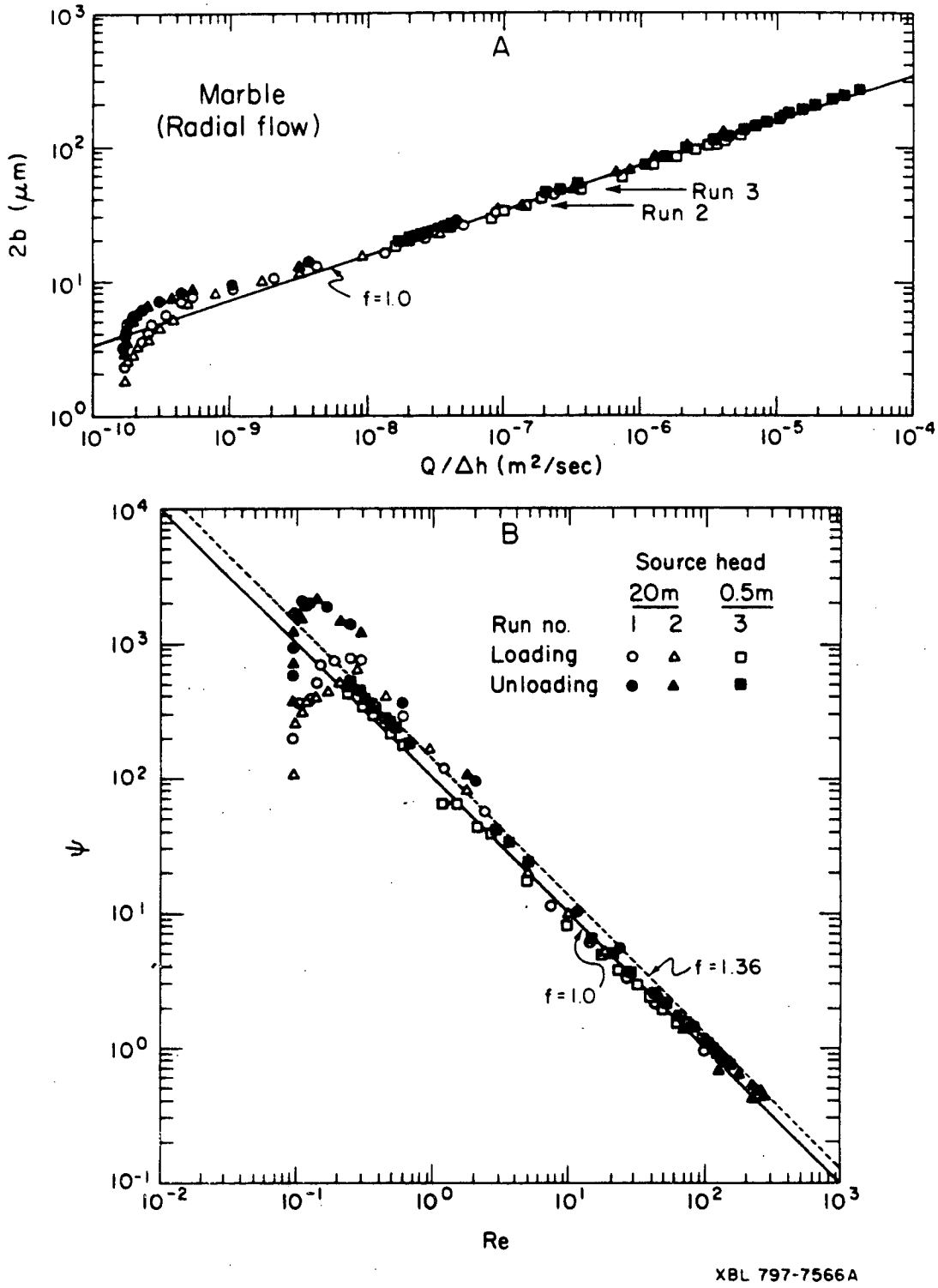

Fig. 8. Comparison of experimental results for radial flow through tension fracture in marble with cubic law. In Runs 2 and 3, fracture surfaces were no longer in contact during unloading when aperture exceeded value indicated by arrow.

Figure C- 4 Marble

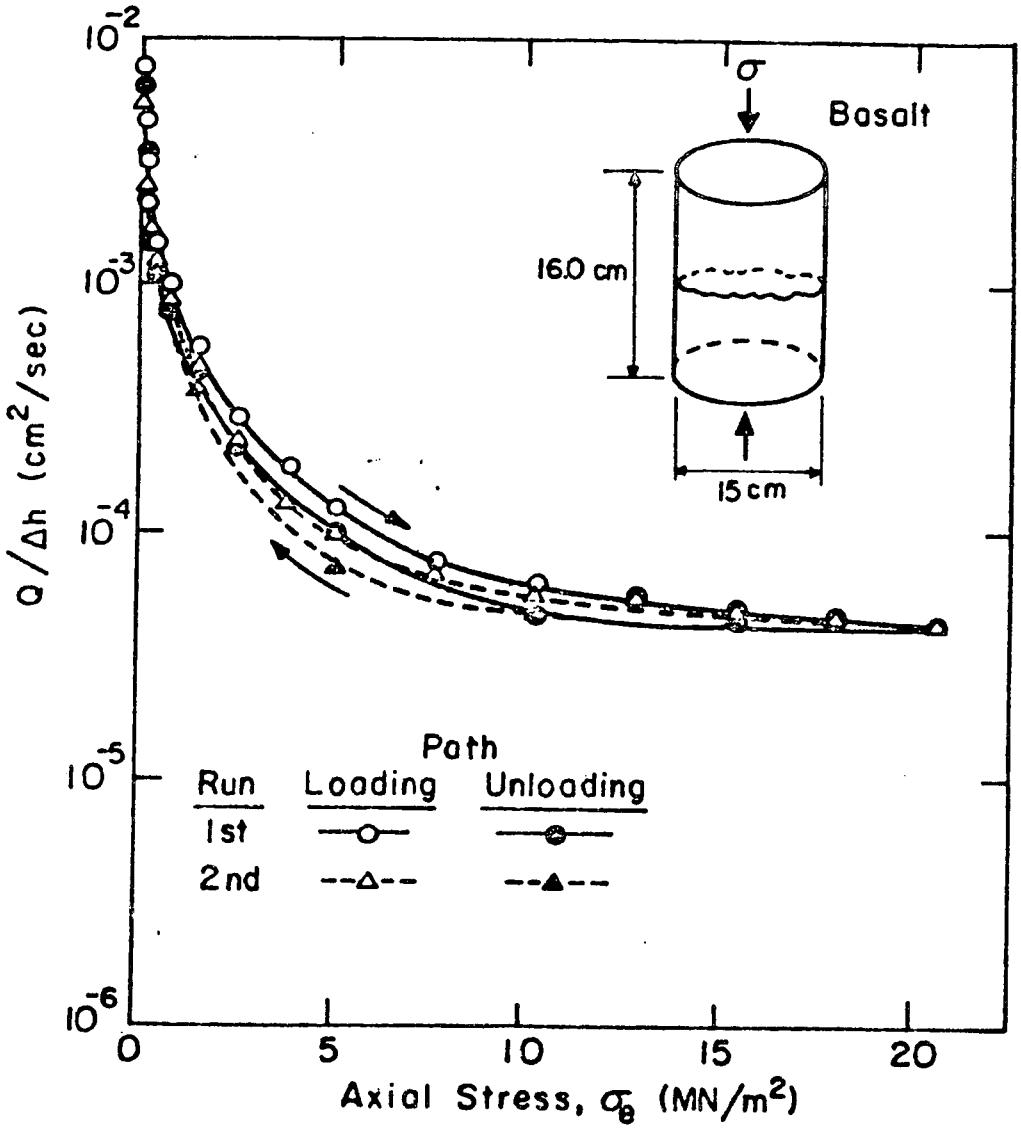

Fig. 4.40. Effect of cyclic loading on permeability of tension fracture in basalt with radial flow.

Figure C-5 Basalt

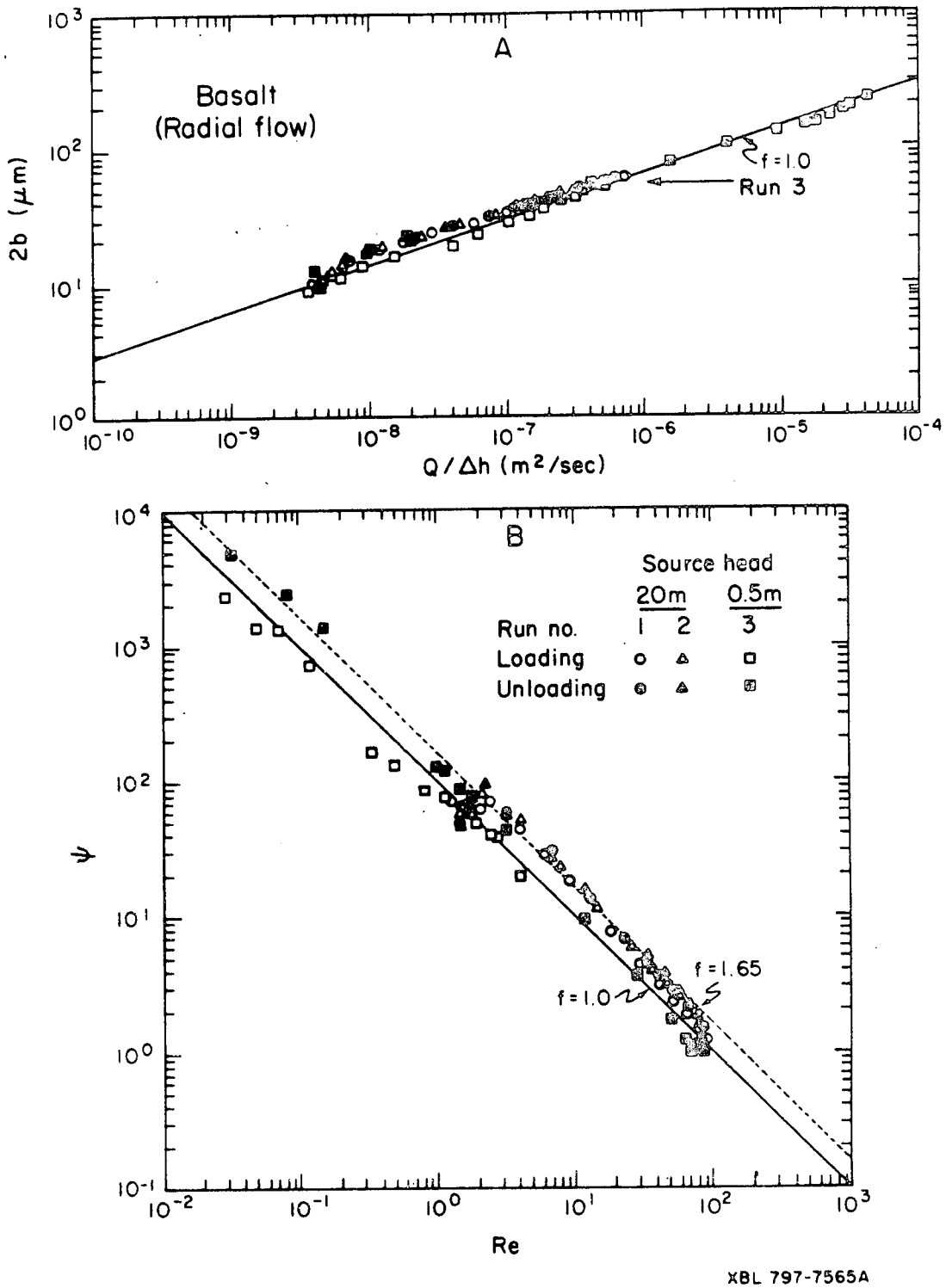

Fig. 7. Comparison of experimental results for radial flow through tension fracture in basalt with cubic law. In Run 3, fracture surfaces were no longer in contact during unloading when aperture exceeded value indicated by arrow.

Figure C- 6 Basalt